Computers and Structures 177 (2016) 114–125

Contents lists available at ScienceDirect

Computers and Structures

journal homepage: www.elsevier.com/locate/compstruc

Bloch wave buckling analysis of axially loaded periodic cylindrical shells

Xin Ning *, Sergio Pellegrino

Graduate Aerospace Laboratories, California Institute of Technology, 1200 E. California Blvd., Pasadena, CA 91125, United States

ARTICLE INFO

Article history:
Received 31 July 2015
Accepted 5 September 2016

Keywords:
Shell buckling
Bloch wave method
Stiffness matrix method
Periodic cylindrical shells

ABSTRACT

This paper presents an efficient computational method for predicting the onset of buckling of axially loaded, corrugated or stiffened cylindrical shells. This method is a modification of the Bloch wave method which builds on the stiffness matrix method. A numerical method and an efficient algorithm have been developed to implement the proposed method in the commercial finite element package Abaqus. Numerical examples have shown that, compared to the nonlinear buckling analyses based on detailed full finite element models, the proposed method can obtain highly accurate buckling loads and buckling modes and can achieve very significant reductions in computational time.

1. Introduction

Commercial finite element codes currently allow the analysis of corrugated and stiffened cylindrical shells; however, detailed simulations are computationally intensive [1]. Typically, the overall dimensions of a cylindrical shell are much larger than the space between stiffeners or the wavelength and amplitude of corrugations. For example, a corrugated shell designed by NASA [2] had a diameter of 3 m, with a corrugation wavelength and amplitude of only 11.4 and 1.1 cm, respectively. Therefore, very small shell elements are needed to accurately mesh the shell geometry, leading to lengthy computations. This high computational effort has been the major constraint on the use of finite element analysis in the optimization of corrugated and stiffened shells [1].

A variety of methods have been introduced to reduce the computational effort required for the buckling analysis of corrugated and stiffened shells. A common approach is to replace their actual shell cross-section with an equivalent, uniform shell. The smeared-out method is a simple method to compute the equivalent properties, and it has been used in the buckling analysis of both corrugated and stiffened shells since the 1960s [2–5]. In this method discrete stiffeners or corrugations are smeared over a smooth surface to replace the original shell geometry with an equivalent, homogeneous orthotropic shell [6].

Motivated by recent studies on corrugated morphing wings, various homogenization methods have been developed to obtain more rigorous equivalent stiffness properties than those provided by the smeared-out method, see Refs. [7–12]. In these methods, strains and curvatures are applied independently on a single corrugation (representative unit cell) and, exploiting the overall periodicity of the structure, the corresponding reaction forces and moments at the boundaries of the unit cell are computed either analytically or numerically. The equivalent stiffness properties of the homogenized shell are then calculated from the load-displacement relations of the representative unit cell.

Both the smeared-out and homogenization methods are effective in reducing significantly the computational effort required by a finite element analysis because a much coarser mesh can be utilized for the analysis, due to the simple geometry of the equivalent shells. However, these two methods are valid only if the shell buckles in a global mode, i.e., only if the buckling wavelength is much longer than the wavelength of the corrugations or the distance between the stiffeners [1,6]. It is well know that these methods cannot be used to capture local skin or stiffener buckling or to calculate stresses in the shell [13].

Axisymmetry of shells of revolution has been exploited in various approaches to reduce computational costs of buckling analyses on such shells. For example, Combescure and co-workers developed special axisymmetric finite elements and used Fourier series analysis to compute critical buckling loads [14–16]. These specific elements can analyze shells with Fourier-mode geometric and thickness imperfections [14,17]. This feature allows buckling analysis on corrugated cylindrical shells, in which corrugations are represented by superposition of several Fourier-mode imperfections. It has been reported that the computational cost of this method is several orders of magnitude lower than general-purpose three-dimensional finite element codes [16]. However, to the best of our knowledge, this method is not available in widely used commercial software and it requires special-purpose elements. It

* Corresponding author.
E-mail address: ningxin87@gmail.com (X. Ning).

http://dx.doi.org/10.1016/j.compstruc.2016.09.006
0045-7949/

should also be noted that corrugations with non-Fourier shapes can only be approximated by superposition of several Fourier modes, which could lead to inaccurate results. Another highly efficient method, called "very large finite element" method, was developed by Steele and co-workers to analyze shells of revolution, in which shells are divided into large sections and then analyzed independently using an asymptotic-numeric approach [18–20]. This method was able to reduce the computational time by a factor of 10 [18]. However, this method also requires special elements and, to the best of our knowledge, has not been applied to shells with intricate corrugations or stiffeners.

An alternative approach to the buckling analysis of corrugated and stiffened shells was developed in the 1980s by Williams and co-workers. These authors developed a stiffness matrix method that treated a shell as an assemblage of flat plates connected along their common longitudinal edges [21–24]. In this method, the stiffness matrix for each plate is computed from flat plate theory, and the buckling loads and buckling modes are obtained by solving an eigenvalue problem. The computer program VIPASA based on this method was found to be much more efficient than general-purpose finite element programs [24,25]. VIPASA can analyze both flat and cylindrical corrugated and stiffened shells.

A unique feature of the stiffness matrix method is that, based on the periodicity of corrugated or stiffened shells, the buckling mode of a repeating portion can be expressed as a product of a complex-valued exponential term times the buckling mode of any repeating portion [26,27]. This relation makes it possible to condense the full stiffness matrix of the whole shell into a smaller matrix related to only a single repeating portion. However, this method can only analyze corrugated and stiffened shells consisting of flat plates. Shells with curved walls, e.g., sinusoidally corrugated shells, must be approximated by a series of flat panels. In addition, it should be noted that in this method the buckling modes are assumed to vary sinusoidally along the corrugations or stiffeners. Therefore, this method could provide inaccurate results if the shells are short and/or clamped in the longitudinal direction.

Another way of exploiting structural periodicity is the Bloch wave method for predicting the onset of buckling of infinitely periodic two- or three-dimensional structures, which was developed in the 1990s by Triantafyllidis and co-workers [28–30]. This method has been one of the major tools for the buckling analysis of cellular structures such as honeycombs [31], porous solids [32], and foams [33]. The Bloch wave method is based on the fact that the buckling modes of an infinitely periodic structure take the form of the Bloch wave propagation, which is the product of a complex-valued plane wave exponential term multiplied by a function with the periodicity of one repeating unit cell [34]. Hence, the buckling loads and corresponding eigenmodes can be computed by performing eigenvalue analyses on a single unit cell whose boundaries are coupled by the Bloch relations rather on the whole structure, resulting in a significant reduction of computational effort. In addition, the Bloch wave method can analyze structures with intricate geometry and materials, such as holes, cut-out, and composites, without using homogenization methods.

In this paper we propose an efficient computational method for predicting the onset of buckling of corrugated/stiffened cylindrical shells subject to axial compression. Our method is a modification of the Bloch wave method based on the stiffness matrix method by Williams and co-workers, to make it applicable for the buckling analysis of rotationally periodic structures. We have implemented the method in the commercial finite element code Abaqus and we have also developed an efficient algorithm to perform the computations.

The paper is organized as follows. Section 2 reviews the stiffness matrix method for rotationally periodic structures and the theory of the Bloch wave method. Section 3 presents the Bloch wave method for corrugated/stiffened cylindrical shells. A method for implementing the proposed method in Abaqus with also an algorithm for computing the critical buckling loads are presented in Section 4. Several example analyses have been carried out with our Bloch wave method, to analyze the buckling behavior of corrugated and stiffened cylindrical shells. The results are presented and compared to nonlinear full finite element analyses in Section 5. Section 6 concludes the paper.

2. Background

This section presents brief reviews of the stiffness matrix method for the buckling analysis of rotationally periodic structures, and the theory of the Bloch wave method for infinitely periodic structures. The similarities and differences between these two methods are also discussed. The reader is referred to Refs. [21–24,26–30] for details of the stiffness matrix method and the Bloch wave method, respectively.

2.1. Stiffness matrix method for rotationally periodic structures

The buckling problem of a rotationally periodic structure can be expressed as an eigenvalue problem:

$$K_c(\lambda_c)\widetilde{U}_c = 0, \tag{1}$$

where K_c is the tangent stiffness matrix of the complete structure, $\widetilde{U}_c$ is an eigenvector, which is also a buckling mode of the structure, and λ_c is the buckling load corresponding to the buckling mode $\widetilde{U}_c$.

For rotationally periodic structures, see the example shown in Fig. 1, with N repeating portions, $\widetilde{U}_c$ can be partitioned into N subsets:

$$\widetilde{U}_c = [\widetilde{U}_1, \widetilde{U}_2, \widetilde{U}_3, \ldots, \widetilde{U}_N]^T, \tag{2}$$

where $\widetilde{U}_q$ is the eigenvector of the qth portion of the structure. The stiffness matrix of a rotational periodic structure has the form [26]:

$$K_c = \begin{bmatrix} K_1 & K_2 & K_3 & \ldots & K_N \\ K_N & K_1 & K_2 & \ldots & K_{N-1} \\ K_{N-1} & K_N & K_1 & \ldots & K_{N-2} \\ \vdots & \vdots & \vdots & \vdots & \vdots \\ K_2 & K_3 & K_4 & \ldots & K_1 \end{bmatrix}, \tag{3}$$

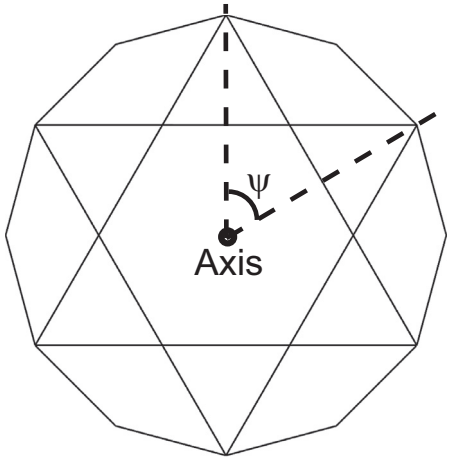

Fig. 1. Rotationally periodic 2D truss structure with 6 repeating portions, $\psi = 2\pi/6$ is the angle subtended by the repeating portion [27].

where K_q is the stiffness matrix corresponding to the qth portion of the structure. Let the number of degrees of freedom of each repeating portion be J, then K_q is a $J \times J$ matrix.

Hence, Eq. (1) can be written as a set of m equations:

$$\sum_{q=1}^{N} K_q(\lambda_c)\widetilde{U}_{m+q-1} = 0, \quad m = 1,2,3,\ldots,N, \tag{4}$$

where

$$\widetilde{U}_{q+N} = \widetilde{U}_q. \tag{5}$$

The most general solution to Eqs. (4) and (5) is [26]:

$$\widetilde{U}_q = \widetilde{U}_1 \exp[i(q-1)n\psi], \quad n = 0,1,2,3,\ldots,N, \tag{6}$$

with $i = \sqrt{-1}, n = 0,1,2,\ldots,N$, and $\psi = 2\pi/N$. Substituting Eq. (6) into Eq. (4) and dividing it by $\exp[imn\psi]$, we can formally reduce the set of m equations to the single equation:

$$\left(\sum_{q=1}^{N} K_q(\lambda_c)\exp[i(q-1)n\psi]\right)\widetilde{U}_1 = 0, \quad n = 0,1,2,3,\ldots,N, \tag{7}$$

which still needs to be solved for each value of n in order to find the smallest value of λ_c.

It should also be noted that, because it is equivalent to define the buckling modes in either an anti-clockwise or clockwise sense around the structure,

$$\exp[i(q-1)(N-n)\psi] = \exp[-i(q-1)n\psi], \tag{8}$$

n and $N-n$ are not independent and the range of n can be reduced to $n = 1,2,3,\ldots,\{N/2\}$, where $\{N/2\}$ is the largest integer no larger than $N/2$.

Thus it has been shown that the eigenvalue problem in Eq. (1), posed in terms of the tangent stiffness matrix of the complete structure, K_c, is equivalent to $\{N/2\}+1$ J-dimensional eigenvalue problems posed in terms of the $\sum_{q=1}^{N} K_q(\lambda_c)\exp[i(q-1)n\psi]$, where J is the size of the stiffness matrix for the repeating portion of the structure.

Here it should be noted that the displacement vector $\widetilde{U}_i$ is complex-valued and hence in general the real and imaginary parts of $\widetilde{U}_i$ are two coincident buckling modes. When $n = 0$ or $n = N/2$ for even N, the exponential term in Eq. (6) is a real value and hence there is only one buckling mode corresponding to these two cases. The critical buckling load is the lowest among the buckling loads for all n's,

$$\lambda_{crit} = \min_{n=0,1,\ldots,\{N/2\}}(\lambda_c(n)). \tag{9}$$

2.2. Bloch wave method for infinitely periodic structures

The Bloch wave method is an efficient way of predicting the onset of buckling for 2-dimensional and 3-dimensional, infinitely periodic structures [28–33]. In this section we use the two-dimensional example shown in Fig. 2 to briefly review this method.

If the structure has not buckled, the periodicity of the structure is still one unit cell in both x- and y-directions, as shown in Fig. 2 (a). When the structure buckles, in general the original periodicity will be broken and a new repeating pattern is found, which could involve several unit cells. Fig. 2(b) shows a buckling mode with a periodicity of 2 unit cells in both x- and y-directions. It has been proved that the buckling modes of a 2-dimensional infinitely periodic structure have the following form [28–30]:

$$\widetilde{U}_c(x,y) = P_u(x,y)\exp\left[2\pi i\left(\frac{n_1}{L_1}x + \frac{n_2}{L_2}y\right)\right], \tag{10}$$

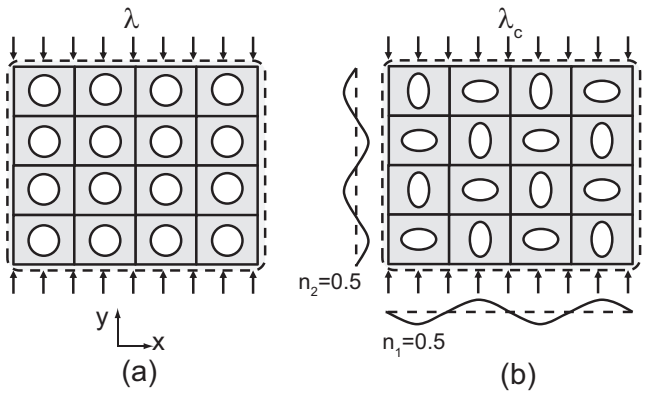

Fig. 2. (a) Schematic of a 2D infinitely periodic porous structure subject to compression in y-direction. (b) A buckling mode and its corresponding buckling load λ_c.

where L_j and $n_j, j = 1,2$ are respectively the lengths of the unit cell and the wave numbers of the buckling modes. $\widetilde{U}_c$ denotes the displacement of the complete infinite structure. $P_u(x,y)$ is a periodic function with a periodicity of one unit cell:

$$P_u(x,y) = P_u(x + m_1L_1, y + m_2L_2), \tag{11}$$

where m_1 and m_2 are integers. Note that both P_u and $\widetilde{U}_c$ are complex-valued functions.

The exponential term in Eq. (10) is essentially a wave propagation term that controls the propagation of P_u. For example, if $n_1 = 0.5$ and $n_2 = 0.5$, the imaginary part of the exponential term follows the sinusoidal waves, as shown in Fig. 2(b), whose wavelength is 2 unit cells in both x- and y-directions. Since the periodicity of P_u is one unit cell, the buckling mode corresponding to $n_1 = n_2 = 0.5$ has a periodicity of two unit cells in both x- and y-directions. Therefore, each value of the wave number n_1 or n_2 represents a buckling mode for the structure in Fig. 2. Eq. (10) is also called the Bloch wave propagation function.

The buckling problem of the infinite structure can be written as an eigenvalue problem, i.e.,

$$K_c(\lambda_c)\widetilde{U}_c = 0, \tag{12}$$

where K_c is the tangent stiffness matrix of the complete structure and λ_c is the buckling load. The above eigenvalue problem cannot be solved due to the infinity of the structure. However, the condition of buckling corresponding to a single unit cell in Fig. 3 can be separated from Eq. (12) and written as:

$$K(\lambda_c)\widetilde{U} = \widetilde{F}, \tag{13}$$

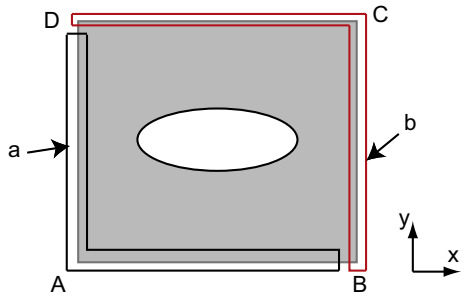

Fig. 3. Schematic of buckled unit cell in a 2D infinitely periodic porous structure, as shown in Fig. 2(b). A, B, C, and D are four points at the corners of the unit cell. Region "a" includes edges AD, AB, and point A; region "b" includes edges CD, BC, and points B, C, and D.

where $\widetilde{U}$ and $\widetilde{F}$ are respectively a buckling mode and corresponding force vector of a unit cell. $K(\lambda_c)$ denotes the tangent stiffness matrix of the unit cell corresponding to the buckling load λ_c. It should be noted that here $\widetilde{F}$ is not zero because we are considering only a piece of the structure, and hence in general non-zero nodal forces need to be applied at the periodic boundaries. Eq. (13) is not an eigenvalue problem and it cannot be directly solved.

The displacements in regions "a" and "b" are not independent. For example, based on Eq. (10), the displacements on edges AD and BC are coupled by the relation:

$$\widetilde{U}_{BC} = \exp[2\pi i n_1]\widetilde{U}_{AD}. \tag{14}$$

Edges AB and CD also follows the similar coupling relation. Eq. (14) is called displacement Bloch relation. The force vector in Eq. (13) also follows the Bloch wave propagation function [28–30]:

$$\widetilde{F}_c(x,y) = P_f(x,y)\exp\left[2\pi i\left(\frac{n_1}{L_1}x + \frac{n_2}{L_2}y\right)\right], \tag{15}$$

where $P_f(x,y)$ is a periodic function with the periodicity of one unit cell. Therefore, the force vectors on edges AD and BC are also coupled:

$$\widetilde{F}_{BC} = -\exp[2\pi i n_1]\widetilde{F}_{AD}. \tag{16}$$

The negative sign is because the reaction forces on edges AD and BC are in opposite directions. Eq. (16) is the force Bloch relation. The details of the Bloch relations are presented in Appendix A.

The dependent displacements can be eliminated by defining a coupling matrix Q:

$$\widetilde{U} = Q[\widetilde{U}_i, \widetilde{U}_a]^T, \tag{17}$$

where i and a denote the internal nodes and the edge nodes in region "a", respectively, as shown in Fig. 3. Q contains the exponential terms in the Bloch relations, and hence it is a function of the wave numbers n_1 and n_2. The derivation of Q is presented in Appendix A.

Substituting Eq. (17) into Eq. (13) and pre-multiplying by Q^T, we obtain:

$$Q^T K(\lambda_c) Q[\widetilde{U}_i, \widetilde{U}_a]^T = Q^T\widetilde{F}. \tag{18}$$

It can be shown that the right-hand-side of Eq. (18) is zero because of the conditions enforced by the force Bloch relations. Hence, we can define the reduced stiffness matrix:

$$\widehat{K}(n_1, n_2, \lambda_c) = Q^T K(\lambda_c) Q \tag{19}$$

and write Eq. (18) as

$$\widehat{K}(n_1, n_2, \lambda_c)[\widetilde{U}_i, \widetilde{U}_a]^T = 0. \tag{20}$$

Therefore, the buckling load λ_c and the corresponding buckling mode can be obtained by solving the eigenvalue problem of matrix $\widehat{K}$. It should be noted that $\widehat{K}$ also depends on n_1 and n_2; hence, the buckling load factor λ_c is a function of n_1 and n_2.

The critical buckling load is obtained by finding the lowest λ_c for all possible n_1 and n_2:

$$\lambda_{crit} = \min_{n_1,n_2}(\lambda_c(n_1,n_2)). \tag{21}$$

For an infinite structure there are infinite values of n_1 and n_2. Therefore, the Bloch wave method is used to find the buckling loads corresponding to the modes with short wavelength. For infinite periodic structures, the buckling modes with very large wavelength are usually analyzed by a homogenization method [32,36].

The practical implementation of this method requires a numerical scheme that can handle complex-valued fields, since the Bloch wave relations and the displacement vectors are complex-valued functions. However, most finite element packages, including Abaqus, cannot handle complex-valued fields. Many authors have formulated the stiffness matrices K and $\widehat{K}$ in Eq. (20) analytically, and then carried out lengthy derivations or developed special purpose software to solve the eigenvalue problems. Gong et al. [33] generated K with the finite element package Abaqus and then obtained $\widehat{K}$ from algebraic manipulations. Åberg and Gudmundson [35] proposed an alternative technique for studying the wave dispersion relations of infinite periodic structures that used two identical meshes in Abaqus to split the complex-valued fields into real and imaginary parts. The boundaries of the two meshes were coupled in order to satisfy the Bloch relations. Following Åberg and Gudmundson [35], Bertoldi et al. introduced this technique in the buckling analysis of porous periodic elastomeric structures [32,36].

Recently, the Bloch wave method was introduced in the buckling analysis of stiffened cylindrical shells by Wang and Abdalla [37]. These authors used the Bloch wave method to find the local buckling loads and buckling modes of stiffened shells (the global buckling modes were analyzed through a homogenized stiffness model). The Bloch wave method for 2-dimensional infinitely periodic structures was used without considering the boundary conditions for the shell, hence assuming the shell to be infinitely long. The constraints of rotational periodicity on the buckling mode were also neglected.

2.3. Comparison between stiffness matrix method and Bloch wave method

The stiffness matrix method for rotationally periodic structures reviewed in Section 2.1 and the Bloch wave method for infinitely periodic structures reviewed in Section 2.2 have similar features. First, both methods achieve significant reductions in computational effort by partitioning the eigenproblem for the whole structure into a series of smaller eigenproblems that involve stiffness matrices with the same dimension as the matrix of a single unit cell. Second, the assumed buckling mode relations among repeating portions of the structure in the stiffness matrix method (Eq. (6)) are essentially the same as the Bloch wave relations in Eq. (14).

However, these two methods formulate the eigenproblems in different ways. The stiffness matrix method involves the stiffness matrices of all the repeating portions of a rotationally periodic structure, as shown in Eq. (7). On the other hand, the stiffness matrix in the Bloch wave method involves only a single unit cell, and the boundaries of the unit cell are coupled by the Bloch wave relations to transform the buckling condition (Eq. (13)) for a unit cell into an eigenproblem, as seen in Eq. (20).

3. New method for axially loaded cylindrical shells

The Bloch wave method has been combined with the stiffness matrix method to develop a new method for rotationally periodic structures. In this section the method is presented using as an example a corrugated cylindrical shell. It should be noted that this method is also applicable to the buckling analysis of stiffened cylindrical shell under axial compression.

3.1. Formulation

Consider, for definiteness, a corrugated cylindrical shell under axial compression. It is periodic only in the circumferential direction and is compressed by the application of a uniform end-shortening on one of its ends, as shown in Fig. 4.

The Bloch wave method for 2-dimensional infinitely periodic structure cannot be directly used for the buckling analysis of axially loaded, rotationally periodic structures, for several reasons.

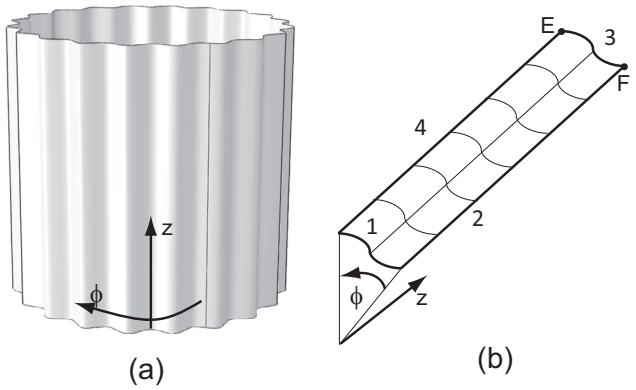

Fig. 4. (a) Corrugated cylindrical shell. (b) Schematic of a complete corrugation. ϕ and z are the circumferential and axial directions, respectively. The four edges of the corrugation are denoted as edges 1–4. E and F are the nodes on the top-left and top-right corners of the corrugation, respectively.

First, the shell is not infinitely long in the longitudinal direction. Second, the Bloch wave method for 2-dimensional infinitely periodic structures cannot capture the effects of clamped boundary conditions on the top and bottom edges in Fig. 4(a). Third, corrugated or stiffened shells have finite number of corrugations or stiffeners in the circumferential direction, leading to finite values of wave numbers in the circumferential direction, as discussed in Section 2.1.

In order to consider the finite length of the shell and the boundary conditions, a complete corrugation, as shown in Fig. 4(b), is considered. Edge 1 is fully clamped and edge 3 is clamped to a rigid plate that is translated in the axial direction, thus applying a uniform end-shortening on the shell. Due to the rotational periodicity, the following Bloch wave propagation functions are used:

$$\begin{aligned}\widetilde{U}(z,\phi) &= P_u(z,\phi)\exp(in\phi)\\ \widetilde{F}(z,\phi) &= P_f(z,\phi)\exp(in\phi),\end{aligned} \tag{22}$$

where z and ϕ denote the shell axial coordinate and angular position in the circumferential direction; n is the wave number. P_u and P_f are rotationally periodic functions with periodicity of one unit cell (one corrugation). Note that there is only one wave number n in the exponential terms corresponding to the wave propagation in the circumferential direction. According to Eq. (22), edges 2 and 4 are coupled by the following displacement and force Bloch relations:

$$\begin{aligned}\widetilde{U}_4 &= \widetilde{U}_2\exp\left(i\frac{2\pi}{N}n\right)\\ \widetilde{F}_4 &= -\widetilde{F}_2\exp\left(i\frac{2\pi}{N}n\right),\end{aligned} \tag{23}$$

where N is the total number of unit cells along the circumferential direction.

We define the coupling matrix $Q(n)$ to eliminate the dependent displacements:

$$\widetilde{U} = QU_{ind}, \tag{24}$$

where U_{ind} contains the independent displacements and $\widetilde{U}_{ind} = [\widetilde{U}_i, \widetilde{U}_1, \widetilde{U}_2, \widetilde{U}_3]^T$. Q consists of the exponential terms in Eq. (23) and hence is a function of wave number n.

Similar to the discussion in Section 2.2, the buckling conditions for a single unit cell can be transformed into the following eigenvalue problem by using the coupling matrix Q:

$$Q^TK(\lambda_c)QU_{ind} = \widehat{K}(n,\lambda_c)U_{ind} = Q^T\widetilde{F} = 0, \tag{25}$$

where λ_c is the buckling load corresponding to the wave number n. More details are presented in Appendix B.

Two features of the stiffness matrix method can be incorporated into the Bloch wave method. First, as discussed in Section 2.1 the feasible values of wave number n are the same as those in the stiffness matrix method:

$$n = 0, 1, 2, \ldots, \{N/2\}, \tag{26}$$

where $\{N/2\}$ is $N/2$ for even N and $(N-1)/2$ for odd N. The displacement relation in Eq. (23) has the same form as Eq. (6). Therefore, n and $N-n$ identify the same mode, but propagating in opposite directions; hence only one of these two terms needs to be included in the analysis. The critical buckling load is the lowest among the buckling loads for all values of n:

$$\lambda_{crit} = \min_{n=0,1,2,\ldots,\{N/2\}}(\lambda_c(n)) \tag{27}$$

Second, the eigenmode has zero displacement on the edge 3 in Fig. 4(b) for $n > 0$. Edge 3 is clamped to a rigid plate and subject to uniform end-shortening. All nodes on edge 3, including nodes E and F, have the same displacements. On the other hand, nodes E and F are also on edges 4 and 2, respectively, and hence their displacements should satisfy the relation in Eq. (23). Therefore, the only condition that satisfies both uniform end-shortening and Eq. (23) is $U_3 = 0$ for $n > 0$. Edge 1 is always fully clamped and U_1 is zero in all analyses.

3.2. Buckling and natural frequency analysis

The eigenvalue problem defined in Eq. (25) is solved by considering the corresponding vibration problem, since buckling happens when the lowest natural frequency of vibration of the structure decreases to zero, as the load magnitude is increased [38].

The equation of motion for a single corrugation is

$$M\ddot{\tilde{u}} + K\tilde{u} = \widetilde{F}, \tag{28}$$

where M and K are the mass and stiffness matrices, respectively. $\tilde{u}$ is the complex-valued displacement field and $\ddot{\tilde{u}}$ denotes its second derivative with respect to time t. The displacement can be written as

$$\tilde{u} = \widetilde{U}e^{i\omega t}, \tag{29}$$

where ω is the angular frequency of vibration. Substitute Eq. (29) into (28), multiply by Q^T, use the relation in Eq. (24), and eliminate the exponential term to obtain the relation:

$$Q^T(K - \omega^2 M)Q\widetilde{U}_a = 0. \tag{30}$$

Eq. (30) is an eigenvalue problem, and the eigenvalue ω^2 and eigenvector $\widetilde{U}$ are respectively the square of the natural frequency and the corresponding vibration mode.

If the lowest natural frequency is zero, i.e. $\omega^2 = 0$, Eq. (30) reduces to the eigenproblem in Eq. (25). Therefore, the buckling problem can be solved by solving the natural frequency problem by finding the load at which the lowest natural frequency is zero. The vibration mode of the frequency problem in this case is also the buckling mode.

When the eigenvalue ω^2 is positive, the angular frequency ω has a real value. Then, $\tilde{u}$ can be written as

$$\tilde{u} = \widetilde{U}e^{i\omega t} = \widetilde{U}(\cos(\omega t) + i\sin(\omega t)). \tag{31}$$

However, when $\omega^2 < 0, \omega$ has a complex value and $e^{i\omega t}$ exponentially grows with time, leading to an unstable structure. Therefore, $\omega^2 = 0$ corresponds to the onset of buckling and this relation is

exploited to facilitate the implementation of the Bloch wave method in the finite element software Abaqus.

4. Numerical implementation

Most existing commercial finite element packages, including Abaqus, cannot deal with complex-valued fields. To implement the Bloch wave method in Abaqus (version 6.12) [39], we have modified the technique developed by Åberg and Gudmundson [35] and Bertoldi et al. [32,36] Our technique is presented in this section, followed by an efficient algorithm for finding critical buckling loads and buckling modes.

4.1. Finite element implementation

Complex-valued fields can be separated into real and imaginary parts, and hence the equation of motion for the free vibration of a single corrugation (Eq. (28)) can be written as

$$\left(\begin{bmatrix} K & \mathbf{0} \\ \mathbf{0} & K \end{bmatrix} - \omega^2 \begin{bmatrix} M & \mathbf{0} \\ \mathbf{0} & M \end{bmatrix}\right) \begin{bmatrix} \widetilde{U}^{Re} \\ \widetilde{U}^{Im} \end{bmatrix} = \begin{bmatrix} \widetilde{F}^{Re} \\ \widetilde{F}^{Im} \end{bmatrix}, \tag{32}$$

where $\widetilde{U}^{Re}, \widetilde{U}^{Im}, \widetilde{F}^{Re}$, and $\widetilde{F}^{Im}$ are the real and imaginary parts of the displacement and force fields for a unit cell. The complex-valued displacement Bloch relation in Eq. (23) can be separated into two equations, each of which represents either a real or an imaginary relation:

$$\begin{aligned} \widetilde{U}_4^{Re} &= \widetilde{U}_2^{Re} \cos\left(\frac{2\pi}{N} n\right) - \widetilde{U}_2^{Im} \sin\left(\frac{2\pi}{N} n\right) \\ \widetilde{U}_4^{Im} &= \widetilde{U}_2^{Re} \sin\left(\frac{2\pi}{N} n\right) + \widetilde{U}_2^{Im} \cos\left(\frac{2\pi}{N} n\right). \end{aligned} \tag{33}$$

Eq. (33) can be represented by two identical meshes in a single analysis in Abaqus whose boundaries are coupled by the *MPC (Multi-Point Constraint) function in Abaqus, as shown in Fig. 5. The displacements of the nodes on edges 2 of the real and imaginary parts are input into Eq. (33) to calculate $\widetilde{U}_4^{Re}$, and then *MPC assigns the obtained value to $\widetilde{U}_4^{Re}$. The imaginary part of the Bloch relations can also be realized in the same way.

In analogy to our previous discussions in Section 3.1, the coupling relations give the following eigenvalue problem:

$$Q^T \left(\begin{bmatrix} K & \mathbf{0} \\ \mathbf{0} & K \end{bmatrix} - \omega^2 \begin{bmatrix} M & \mathbf{0} \\ \mathbf{0} & M \end{bmatrix}\right) Q \widetilde{U}_{ind} = 0, \tag{34}$$

where $\widetilde{U}_{ind}$ contains the independent displacements and Q is the coupling matrix. More details can be found in Appendix B.

The calculation of ω^2 consists of two steps: a nonlinear static analysis (pre-buckling analysis) and a frequency analysis (eigenvalue analysis). In the static analysis the pre-buckling deformation of the cylindrical shell has the periodicity of one unit cell, which is enforced by setting $\widetilde{U}_2^{Re} = \widetilde{U}_4^{Re}$ and $\widetilde{U}_2^{Im} = \widetilde{U}_4^{Im}$. Edge 1 is fully clamped and the shell is compressed by applying a uniform axial end-shortening on edge 3, i.e., $\widetilde{U}_1^{Re} = \widetilde{U}_1^{Im} = 0$ and $\widetilde{U}_{z,3}^{Re} = \widetilde{U}_{z,3}^{Im} = U_z$. Therefore, the load parameter λ is $\lambda = |U_z|$.

In the frequency analysis the stress state obtained from the previous nonlinear static analysis is kept unchanged, and edges 2 and 4 are coupled by the Bloch relations in Eq. (33). Edge 1 is fully clamped. Edge 3, as discussed in Section 3.1, is subject to the boundary conditions $\widetilde{U}_3^{Re} = 0$ and $\widetilde{U}_3^{Im} = 0$ when $n > 0$, in order to satisfy the Bloch relations. For the case $n = 0$, the real and imaginary parts are not coupled and the only free degree of freedom of edge 3 is the uniform translational displacement in the z (axial) direction. The particular value of $|U_z|$ corresponding to $\omega^2 = 0$ is λ_c for the wave number n.

4.2. Algorithm for finding critical buckling load

In principle, according to Eq. (27), we need to analyze $\{N/2\} + 1$ buckling modes in order to find the critical buckling mode which has the lowest buckling load:

$$\lambda_{crit} = \min_{n=0,1,2,\ldots,\{N/2\}} (\lambda_c(n))$$

The number of simulations required to find the lowest buckling load is reduced by the algorithm shown in Fig. 6. In this algorithm, the buckling modes are not sequentially analyzed; instead, after analyzing the first buckling mode $n = 0$, a possible critical buckling mode is iteratively identified and analyzed. The iteration is stopped when the possible critical buckling mode is found to be the critical buckling mode.

4.2.1. Calculating the buckling load for mode $n = 0$

Calculating the buckling load for mode $n = 0$ consists of a geometrically nonlinear static analysis step followed by a frequency analysis step, as discussed in Section 4.1. The buckling load is found when the eigenvalue ω^2 obtained from the frequency analysis is zero.

In the nonlinear static step, the shell is compressed by incrementally applying a uniform end-shortening. In order to reduce the computational time, coarse increments are first used, and then

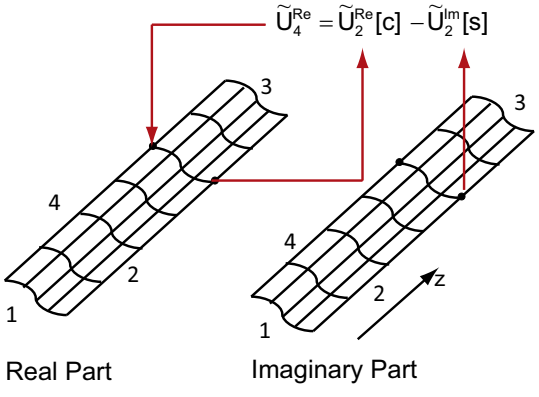

Fig. 5. Schematic of two identical meshes coupled by the *MPC function in Abaqus. [s] and [c] are the sine and cosine terms in Eq. (33), respectively. Only the real part of the Bloch relation is shown in this figure.

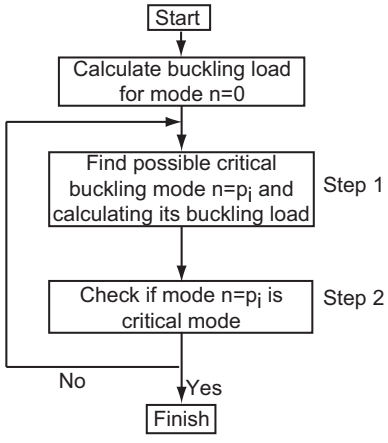

Fig. 6. Flow chart of algorithm for finding the critical buckling mode and load.

the increment containing the buckling point ($\omega^2 = 0$) is refined until the required accuracy is achieved. The frequency analyses are independent, so they are carried out in parallel to further reduce the computational time.

The iterative loop consists of two steps which are described next.

4.2.2. Step 1

The frequency analyses based on a certain stress state produce positive ω^2 for some modes and negative ω^2 for others. The buckling modes with positive ω^2 are guaranteed not to be the critical mode, because they require larger loads to make ω^2 decrease to zero. Therefore, modes with positive ω^2 are discarded in future analyses. The critical buckling mode is among the modes with negative ω^2, and we choose the one with smallest ω^2 as the possible critical mode, denoted as p_i for the ith iteration.

For the first iteration, the stress state corresponding to the buckling load for the mode $n = 0$ is used to find the possible critical mode. For the ith ($i > 1$) iteration, the stress state corresponding to the buckling load of the previous possible critical mode $n = p_{i-1}$ is used. We use the same technique as the $n = 0$ mode to find the buckling load for the mode $n = p_{i-1}$, which is denoted as $\lambda_c(p_i)$.

4.2.3. Step 2

If $n = p_i$ is the critical mode which corresponds to the lowest buckling load, then the eigenvalues ω^2 for the other modes corresponding to the stress state at $\lambda_c(p_i)$ are all positive. The iteration is stopped when this criterion is satisfied.

This algorithm can reduce computational effort due to three reasons. First, it always finds the buckling load of the possible critical mode rather than sequentially searches $n = 0, 1, 2, \ldots, \{N/2\}$. Hence, it can find the critical mode as soon as possible. Second, coarse increments are first used and the increment containing the bifurcation point is then refined in the static analysis. This can reduce the number of nonlinear analyses which are time-consuming. Third, independent frequency analyses are carried out in parallel, further reducing the computational time.

5. Numerical examples

The analysis method presented in this paper has been applied to several corrugated cylindrical shells and a stiffened cylindrical shell in order to validate both the method formulation and the implementation techniques. For each problem, an additional solution was obtained by carrying out nonlinear buckling analyses using full finite element models, i.e., using complete structural models with the same mesh refinement used in the Bloch wave method. Note that a nonlinear buckling analysis is an eigenvalue analysis of a loaded structure whose stress state is obtained by a geometrically nonlinear static analysis. The results and computational times required for the full nonlinear analyses are compared to the proposed method.

5.1. Corrugated composite cylindrical shells

5.1.1. Shell geometry and material

The corrugations are sinusoidal and the cross-sections were obtained by superposing the sinusoidal wave on a reference circle:

$$r(\phi) = R + \Delta r \sin(N\phi), \tag{35}$$

where N is the total number of corrugations and Δr their amplitude. The values of N were chosen to be 12, 13, 16, 17, 19, 22, 23, 34, 25, 26, 29, 30, 31, 37, and 40, in order to consider shells with odd, even and prime numbers of corrugations.

The shells were chosen to have a square aspect ratio; their dimensions are presented in Table 1.

A symmetric six-ply laminate, $[+60^\circ, -60^\circ, 0^\circ]_s$ was adopted, where the 0° direction is the axial direction of the shell. The laminate consisted of 30 μm thick unidirectional laminae of T800 carbon fibers and ThinPreg 120EPHTg-402 epoxy, with a fiber volume fraction of 50%. The following lamina properties were $E_1 = 127.9$ GPa, $E_2 = 6.49$ GPa, $G_{12} = 7.62$ GPa, and $\nu_{12} = 0.354$, where E_1 is the modulus along the fiber direction. The ABD matrix of the laminate was calculated from these properties, using classical lamination theory [40]:

$$ABD = \begin{pmatrix} 9.919\times10^6 & 2.670\times10^6 & 0 & 0 & 0 & 0 \\ 2.670\times10^6 & 9.919\times10^6 & 0 & 0 & 0 & 0 \\ 0 & 0 & 3.625\times10^6 & 0 & 0 & 0 \\ 0 & 0 & 0 & 0.0108 & 0.0099 & 0.0034 \\ 0 & 0 & 0 & 0.0099 & 0.0373 & 0.0081 \\ 0 & 0 & 0 & 0.0034 & 0.0081 & 0.0125 \end{pmatrix} \tag{36}$$

where the units of the A and D matrices are N/m and Nm, respectively.

5.1.2. Buckling loads and modes

All simulations of the sinusoidally corrugated shells were run on a Xeon X5680 server with 12 CPUs on a single motherboard. Around 1500 S4 fully integrated shell elements were used for a single corrugation. The full finite element models have the same element size as the models in the Bloch wave method.

The full nonlinear analyses consisted of two steps, similar to the Bloch wave method, i.e., a nonlinear static analysis and a frequency analysis. The shells were first compressed by applying a uniform end-shortening at one end, and then a frequency step was carried out to find the eigenvalue ω^2 corresponding to this stress state. The critical buckling load was found when the eigenvalue ω^2 decreased to zero. Coarse increments in the nonlinear static step were first used and the increment containing the bifurcation point was then refined. Each frequency analysis is independent and hence the frequency analyses were performed in parallel.

The results obtained from the Bloch wave method are compared to the results obtained from the nonlinear full finite element analyses. Figs. 7 and 8 show that the results obtained from the three methods are practically coincident. It was found that the differences were less than 0.5% for all the corrugated shells studied in this paper.

The buckling modes obtained from the Bloch wave method and nonlinear full model analysis for $N = 13, 31$ are plotted in Figs. 9 and 10. The buckling modes in Fig. 9 are typical for shells with $N \leqslant 30$ corrugations. Each corrugation buckled into several half waves in the axial direction and two half waves in the circumferential direction. The size of the representative unit cell of the structure, i.e., a corrugation, is larger than the buckling wavelength in both axial and circumferential directions. Therefore, the buckling modes are local for $N \leqslant 30$. Fig. 9 shows that the Bloch wave method can accurately capture the local buckling modes. The differences between Fig. 9(a) and (b) are very small.

Fig. 10(a) and (b) shows typical buckling modes for shells with $N \geqslant 31$ corrugations. In this case, there is only one half wave in the axial direction. The most significant component of the buckling mode is a uniform expansion in the radial direction. Therefore,

Table 1
Dimensions of sinusoidally corrugated shells.

Thickness, t	180 μm
Radius, R	35 mm
Length L	70 mm
Maximum deviation from circle, Δr	1.5 mm

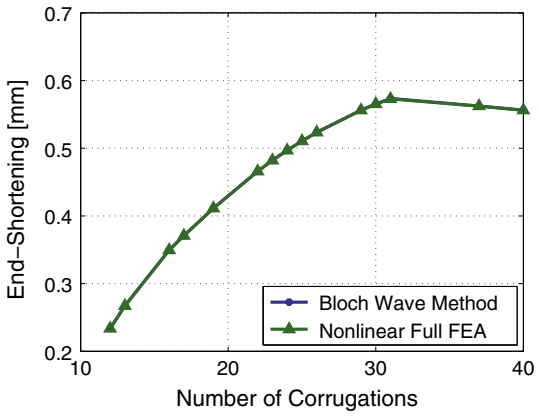

Fig. 7. Critical end-shortening obtained from Bloch wave method and nonlinear full FEA models.

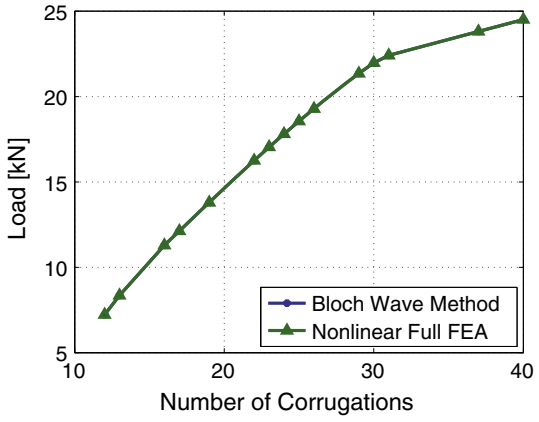

Fig. 8. Critical buckling loads obtained from Bloch wave method and nonlinear full FEA models.

the buckling modes for $N \geqslant 31$ are global. Fig. 10 shows that, compared to the nonlinear full FEA, the Bloch wave method can obtain accurate global buckling modes.

Considering all of the above results, it has been shown that the Bloch wave method captures both local (short wavelength) and global (long wavelength) buckling and the buckling modes match almost exactly the results obtained from the nonlinear full model analyses.

5.1.3. Computational time

The computational time for the two sets of simulations is plotted in Fig. 11. It can be seen that the computational time of the nonlinear full FEA models increased linearly with respect to the number of corrugations. However, the computational time of the Bloch wave method did not significantly change as the number of corrugations was increased.

5.2. Orthogonally stiffened aluminum cylindrical shell

5.2.1. Shell geometry and material

We applied the Bloch wave method to the computation of the critical buckling load and the buckling mode of a large orthogonally stiffened aluminum cylindrical shell which was recently constructed by NASA for the Shell Buckling Knockdown Factor project [41]. The stiffeners are on the internal side of the shell and consist of longitudinal stringers and circumferential rings, as shown in Fig. 12. The dimensions are listed in Table 2. The shell has 75 longitudinal stringers and 18 circumferential rings. Since the material properties were not included in Ref. [41], the modulus and Poisson's ratio used in the present study were chosen to be 68.9 GPa and 0.3, respectively.

5.2.2. Buckling loads, modes, and computational time

The unit cell shown in Fig. 13 was used for the Bloch wave method analysis. All simulations of these examples were run on a Xeon E5410 desktop with 8 CPUs. Around 1100 S4 fully integrated shell elements were used for a unit cell in the Bloch wave analysis. The full FEA models had the same element type and size as the Bloch wave method.

The buckling loads obtained from the two simulations and their computational time are presented in Table 3. Compared to the full nonlinear FEA model, the errors in the critical end-shortening obtained from the Bloch wave method are within 0.3%. The difference between the buckling loads of the full nonlinear FEA model and the Bloch wave method is within 0.6%. Although the full nonlinear FEA model was slightly more accurate, it took 16 h to complete.

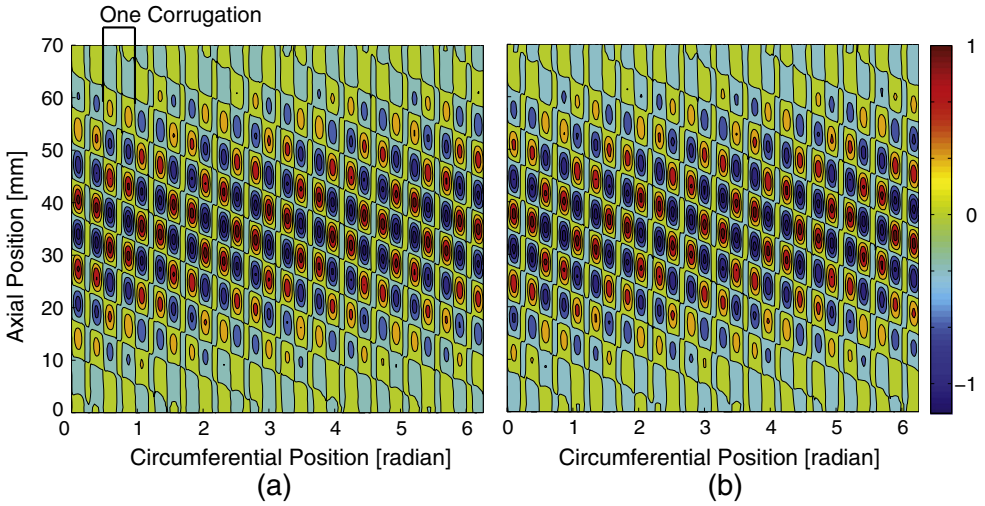

Fig. 9. Normalized buckling modes of the shell with $N = 13$ corrugations obtained from (a) Bloch wave method and (b) nonlinear full FEA model.

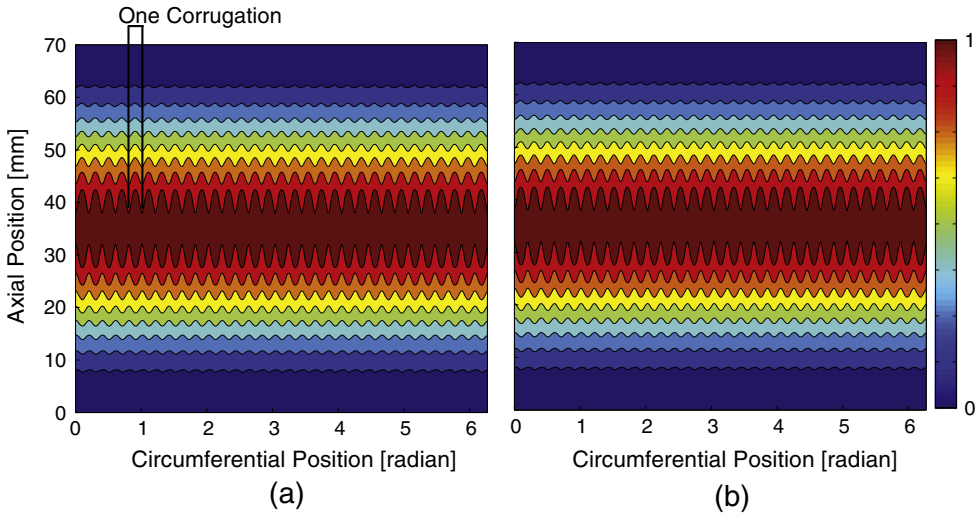

Fig. 10. Normalized buckling modes of the shell with $N = 31$ corrugations obtained from (a) Bloch wave method and (b) nonlinear full FEA model.

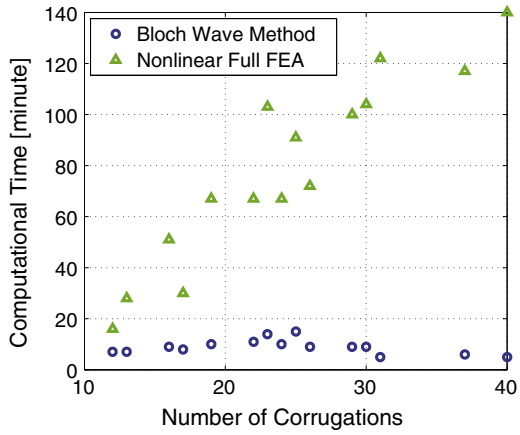

Fig. 11. Computation time for Bloch wave method and nonlinear full FEA models.

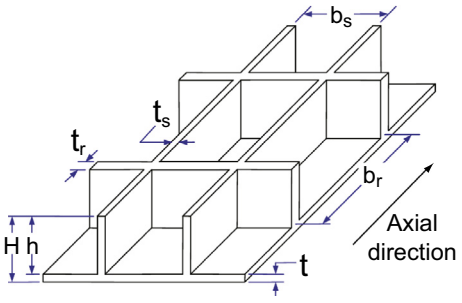

Fig. 12. Schematic of stiffeners (from Ref. [41]).

Table 2
Dimensions of stiffeners (from Ref. [41]). Units are inches.

Skin thickness, t	0.100
Stiffener height, H	0.400
Stiffener height, h	0.300
Space between stringers, b_s	4.00
Stringer thickness, t_s	0.100
Space between rings, b_r	4.00
Ring thickness, t_r	0.100
Shell radius, R	48.0
Shell length, L	72.0

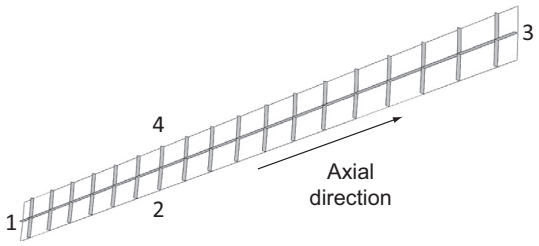

Fig. 13. Schematic of unit cell used in the Bloch wave method analysis.

Table 3
Critical end-shortening (U_{cr}), critical axial load (F_{cr}), and computational time (T) of stiffened cylindrical shell.

	U_{cr} [mm]	F_{cr} [kN]	T [h]
Bloch wave method	3.3546	2719	0.5
Full nonlinear FEA	3.3554	2702	16

The buckling modes obtained from the Bloch wave method and nonlinear full model analysis for the stiffened shell are plotted in Fig. 14(a) and (b). It can be seen that the Bloch wave method produces accurate buckling mode. The buckling mode has 5 half waves in the axial direction. There are 15 waves in the circumferential direction and each circumferential full wave spans over 5 stringers. Compared to the size of the grid in Fig. 12, the wavelength in both axial and circumferential directions is larger.

6. Conclusion

We have developed an efficient computational method for the buckling analysis of corrugated and stiffened cylindrical shells which builds on the Bloch wave method and the stiffness matrix method for rotationally periodic structures. The traditional Bloch wave method is applicable for the buckling analysis of infinitely 2- or 3-dimensional periodic structures. We modified the Bloch wave method in order to analyze the buckling of rotationally periodic shell structures subject to axial compression. We implemented our Bloch wave method in the commercial finite element code Abaqus, following Refs. [32,35,36], and also developed a

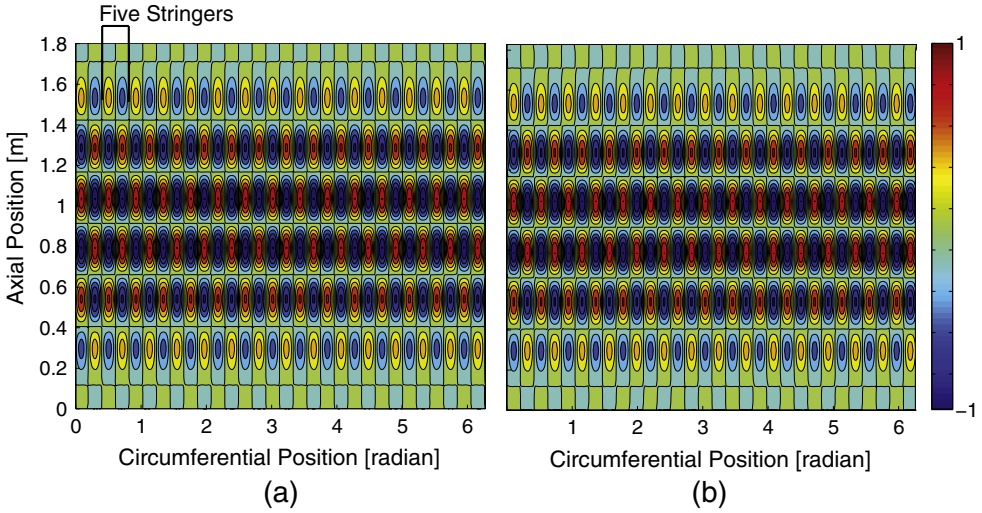

Fig. 14. Normalized buckling modes of the stiffened shell obtained from (a) Bloch wave method and (b) nonlinear full FEA model.

highly efficient algorithm of performing the evaluation of critical buckling load and buckling mode.

We used the Bloch wave method to analyze the onset of buckling for several small corrugated composite cylindrical shells and a large-scale orthogonally stiffened aluminum cylindrical shell. Nonlinear analyses based on full, detailed finite element models were also performed in order to validate our method. It was shown that our method provides highly accurate buckling loads. Compared to the nonlinear full FEA models, the errors of the buckling loads obtained by the Bloch wave method are smaller than 0.6% for all the shells studied in this paper. These examples also show that the Bloch wave method produces almost exactly the same buckling modes as those obtained from the nonlinear full FEA models and that it can accurately capture local (short wavelength) and global (long wavelength) buckling modes.

In the examples of corrugated cylindrical shells, the computational time required by the Bloch wave method did not significantly change when the number of corrugations was increased. However, the nonlinear full FEA models required much longer computational time than the Bloch wave method for heavily corrugated shells. For a shell with 40 corrugations, the computational time of the Bloch wave method is only 7% of the computational time of the nonlinear full FEA models. For the stiffened cylindrical shell, the computational time of the Bloch wave method is only 3% of the computational time of the nonlinear full FEA models.

It should be noted that our method does not require special-purpose elements and is compatible with Abaqus, a widely used commercial finite element software. Moreover, the reduction in computational time can be achieved without any homogenization or approximation on the shell geometry. In addition, our method only requires coupling between boundaries of a repeating unit and does not limit the geometry in the internal part of a unit. Therefore, it can analyze periodic cylindrical shells with intricate geometries, such as cutout, non-continuous or curved stiffeners, and complex corrugations, as long as the geometric features are periodic. Due to these advantages, our method has potential in buckling analyses on complex periodic cylindrical shells that require high accuracy and efficiency.

The savings achieved in the present study are very promising. However, it should be noted the Bloch wave method has been applied only to identically repeating unit cells. However, practical imperfections are usually not periodic and their wavelength may be much larger than a repeating unit cell. In the future it would be worth investigating the Bloch wave method for imperfect or nearly perfect structures.

Acknowledgments

We thank Dr. Katia Bertoldi for providing her presentations at the 2014 CISM course on Extremely Deformable Structures. We also thank Drs. Francisco López Jiménez and Ryan Elliott for helpful discussions on the Bloch wave method.

Appendix A. Bloch relations and coupling matrix for a 2-dimensional infinite periodic structure

$\widetilde{U}$ and $\widetilde{F}$ in Eq. (13) can be separated into the values on boundary and internal nodes:

$$\begin{aligned}\widetilde{U} &= [\widetilde{U}_i, \widetilde{U}_a, \widetilde{U}_b]^T \\ \widetilde{F} &= [\widetilde{F}_i, \widetilde{F}_a, \widetilde{F}_b]^T\end{aligned} \tag{A.1}$$

where i, a and b denote the internal nodes, nodes in regions "a" and "b", respectively, as shown in Fig. 3. Therefore, the displacements and forces of regions "a" and "b" are:

$$\begin{aligned}\widetilde{U}_a &= [\widetilde{U}_{(AD)}, \widetilde{U}_A, \widetilde{U}_{(AB)}]^T \\ \widetilde{F}_a &= [\widetilde{F}_{(AD)}, \widetilde{F}_A, \widetilde{F}_{(AB)}]^T \\ \widetilde{U}_b &= [\widetilde{U}_B, \widetilde{U}_{(BC)}, \widetilde{U}_C, \widetilde{U}_{(CD)}]^T \\ \widetilde{F}_b &= [\widetilde{F}_B, \widetilde{F}_{(BC)}, \widetilde{F}_C, \widetilde{F}_{(CD)}]^T\end{aligned} \tag{A.2}$$

The notation $(*)$ means edges without their end nodes.

Using Eqs. (10) and (15), we can obtain the following Bloch relations for the displacements on the boundary nodes:

$$\begin{aligned}&U_B = \mu_1 U_A; \quad U_{(BC)} = \mu_1 U_{(AD)}; \quad U_C = \mu_1 U_D; \\ &U_C = \mu_2 U_B; \quad U_{(CD)} = \mu_2 U_{(AB)}; \quad U_D = -\mu_2 U_A\end{aligned} \tag{A.3}$$

where $\mu_1 = \exp(2\pi i n_1)$ and $\mu_2 = \exp(2\pi i n_2)$. Similarly, the forces on the boundaries have the following Bloch relations:

$$\begin{aligned}&F_B = -\mu_1 F_A; \quad F_{(BC)} = -\mu_1 F_{(AD)}; \quad F_C = -\mu_1 F_D; \\ &F_C = -\mu_2 F_B; \quad F_{(CD)} = -\mu_2 F_{(AB)}; \quad F_D = -\mu_2 F_A\end{aligned} \tag{A.4}$$

Using Eq. (A.3), the displacements can be written as:

$$[\widetilde{U}_i, \widetilde{U}_{(AD)}, \widetilde{U}_A, \widetilde{U}_{(AB)}, \widetilde{U}_B, \widetilde{U}_{(BC)}, \widetilde{U}_C, \widetilde{U}_{(CD)}]^T = Q[\widetilde{U}_i, \widetilde{U}_{(AD)}, \widetilde{U}_A, \widetilde{U}_{(AB)}]^T \tag{A.5}$$

where the transformation matrix Q is defined as:

$$Q = \begin{bmatrix} \mathbf{I} & \mathbf{0} & \mathbf{0} & \mathbf{0} \\ \mathbf{0} & \mathbf{I} & \mathbf{0} & \mathbf{0} \\ \mathbf{0} & \mathbf{0} & \mathbf{I} & \mathbf{0} \\ \mathbf{0} & \mathbf{0} & \mathbf{0} & \mathbf{I} \\ \mathbf{0} & \mathbf{0} & [\mu_1] & \mathbf{0} \\ \mathbf{0} & [\mu_1] & \mathbf{0} & \mathbf{0} \\ \mathbf{0} & \mathbf{0} & [\mu_1\mu_2] & \mathbf{0} \\ \mathbf{0} & \mathbf{0} & \mathbf{0} & [\mu_2] \end{bmatrix} \tag{A.6}$$

The notation $[*]$ represents a diagonal submatrix with entries equal to $*$.

Appendix B. Bloch relations and coupling matrix of a rotationally periodic structure

$\widetilde{U}$ and $\widetilde{F}$ in Eqs. (24) and (25) can be separated into the values on boundary and internal nodes:

$$\begin{aligned} \widetilde{U} &= [\widetilde{U}_i, \widetilde{U}_{(1)}, \widetilde{U}_{[2]}, \widetilde{U}_{(3)}, \widetilde{U}_{[4]}]^T \\ \widetilde{F} &= [\widetilde{F}_i, \widetilde{F}_{(1)}, \widetilde{F}_{[2]}, \widetilde{F}_{(3)}, \widetilde{F}_{[4]}]^T \end{aligned} \tag{B.1}$$

The notations $(*)$ and $[*]$ represent edges respectively without and with their end nodes. The equilibrium equation of a corrugation on the point of buckling is

$$K(\lambda_c)[\widetilde{U}_i, \widetilde{U}_{(1)}, \widetilde{U}_{[2]}, \widetilde{U}_{(3)}, \widetilde{U}_{[4]}]^T = [\widetilde{F}_i, \widetilde{F}_{(1)}, \widetilde{F}_{[2]}, \widetilde{F}_{(3)}, \widetilde{F}_{[4]}]^T \tag{B.2}$$

The stiffness matrix $K(\lambda_c)$ and force vector $[\widetilde{F}_i, \widetilde{F}_{(1)}, \widetilde{F}_{[2]}, \widetilde{F}_{(3)}, \widetilde{F}_{[4]}]^T$ in Eq. (B.2) can be assembled into the global stiffness and force vector of the whole corrugated shell, and the following eigenproblem is then obtained:

$$K_c(\lambda)\widetilde{U}_c = \widetilde{F}_c = 0 \tag{B.3}$$

where K_c and $\widetilde{U}_c$ are the global stiffness matrix and the eigenvector of the whole structure.

$\widetilde{F}_c$ is zero when the structure buckles. Note that the force vectors $F_i, F_{(1)}$, and $F_{(3)}$ remain unchanged when they are assembled into the force vector in Eq. (B.3) because the edges (1), (3), and internal nodes do not interact with the nodes in other corrugations. Therefore, Eq. (B.2) can be written as:

$$K(\lambda)[\widetilde{U}_i, \widetilde{U}_{(1)}, \widetilde{U}_{[2]}, \widetilde{U}_{(3)}, \widetilde{U}_{[4]}]^T = [0, 0, \widetilde{F}_{[2]}, 0, \widetilde{F}_{[4]}]^T \tag{B.4}$$

The incremental displacements on edge 4 can be eliminated by means of the relation:

$$[\widetilde{U}_i, \widetilde{U}_{(1)}, \widetilde{U}_{[2]}, \widetilde{U}_{(3)}, \widetilde{U}_{[4]}]^T = Q[\widetilde{U}_i, \widetilde{U}_{(1)}, \widetilde{U}_{[2]}, \widetilde{U}_{(3)}]^T \tag{B.5}$$

where Q is

$$Q = \begin{bmatrix} \mathbf{I} & \mathbf{0} & \mathbf{0} & \mathbf{0} \\ \mathbf{0} & \mathbf{I} & \mathbf{0} & \mathbf{0} \\ \mathbf{0} & \mathbf{0} & \mathbf{I} & \mathbf{0} \\ \mathbf{0} & \mathbf{0} & \mathbf{0} & \mathbf{I} \\ \mathbf{0} & \mathbf{0} & [\exp(i\frac{2\pi}{N}n)] & \mathbf{0} \end{bmatrix} \tag{B.6}$$

Letting $[U_i, U_{(1)}, U_{[2]}, U_{(3)}]^T = \widetilde{U}_{ind}$, and proceeding in analogy to Eqs. (18)–(20), we obtain the following eigenproblem:

$$Q^T K(\lambda) Q \widetilde{U}_{ind} = \widehat{K}(n,\lambda)\widetilde{U}_{ind} = Q^T\widetilde{F} = 0, \quad n = 0, 1, 2, \ldots, \{N/2\} \tag{B.7}$$

where λ is the loading factor.

The transformation matrix Q can also be separated into real and imaginary parts, based on Eq. (33):

$$\begin{bmatrix} U_i^{Re} \\ U_{(1)}^{Re} \\ U_{[2]}^{Re} \\ U_{(3)}^{Re} \\ U_{[4]}^{Re} \\ U_i^{Im} \\ U_{(1)}^{Im} \\ U_{[2]}^{Im} \\ U_{(3)}^{Im} \\ U_{[4]}^{Im} \end{bmatrix} = Q \begin{bmatrix} U_i^{Re} \\ U_{(1)}^{Re} \\ U_{[2]}^{Re} \\ U_{(3)}^{Re} \\ U_i^{Im} \\ U_{(1)}^{Im} \\ U_{[2]}^{Im} \\ U_{(3)}^{Im} \end{bmatrix} \tag{B.8}$$

where the Q matrix is

$$\begin{bmatrix} \mathbf{I} & \mathbf{0} & \mathbf{0} & \mathbf{0} & \mathbf{0} & \mathbf{0} & \mathbf{0} & \mathbf{0} \\ \mathbf{0} & \mathbf{I} & \mathbf{0} & \mathbf{0} & \mathbf{0} & \mathbf{0} & \mathbf{0} & \mathbf{0} \\ \mathbf{0} & \mathbf{0} & \mathbf{I} & \mathbf{0} & \mathbf{0} & \mathbf{0} & \mathbf{0} & \mathbf{0} \\ \mathbf{0} & \mathbf{0} & \mathbf{0} & \mathbf{I} & \mathbf{0} & \mathbf{0} & \mathbf{0} & \mathbf{0} \\ \mathbf{0} & \mathbf{0} & [\cos(\frac{2\pi}{N}n)] & \mathbf{0} & \mathbf{0} & \mathbf{0} & -[\sin(\frac{2\pi}{N}n)] & \mathbf{0} \\ \mathbf{0} & \mathbf{0} & \mathbf{0} & \mathbf{0} & \mathbf{I} & \mathbf{0} & \mathbf{0} & \mathbf{0} \\ \mathbf{0} & \mathbf{0} & \mathbf{0} & \mathbf{0} & \mathbf{0} & \mathbf{I} & \mathbf{0} & \mathbf{0} \\ \mathbf{0} & \mathbf{0} & \mathbf{0} & \mathbf{0} & \mathbf{0} & \mathbf{0} & \mathbf{I} & \mathbf{0} \\ \mathbf{0} & \mathbf{0} & \mathbf{0} & \mathbf{0} & \mathbf{0} & \mathbf{0} & \mathbf{0} & \mathbf{I} \\ \mathbf{0} & \mathbf{0} & [\sin(\frac{2\pi}{N}n)] & \mathbf{0} & \mathbf{0} & \mathbf{0} & [\cos(\frac{2\pi}{N}n)] & \mathbf{0} \end{bmatrix} \tag{B.9}$$

The Bloch relations for the forces are:

$$\begin{aligned} \widetilde{F}_{[4]}^{Re} &= -\left(\widetilde{F}_{[2]}^{Re}\cos\left(\frac{2\pi}{N}n\right) - \widetilde{F}_{[2]}^{Im}\sin\left(\frac{2\pi}{N}n\right)\right) \\ \widetilde{F}_{[4]}^{Im} &= -\left(\widetilde{F}_{[2]}^{Re}\sin\left(\frac{2\pi}{N}n\right) + \widetilde{F}_{[2]}^{Im}\cos\left(\frac{2\pi}{N}n\right)\right) \end{aligned} \tag{B.10}$$

We can also obtain the following relation by multiplying Eq. (32) by Q^T and using the above force Bloch relations and $F_i = 0, F_{(1)} = 0$, and $F_{(3)} = 0$:

$$Q^T\left(\begin{bmatrix} K & \mathbf{0} \\ \mathbf{0} & K \end{bmatrix} - \omega^2\begin{bmatrix} M & \mathbf{0} \\ \mathbf{0} & M \end{bmatrix}\right)Q \begin{bmatrix} U_i^{Re} \\ U_{(1)}^{Re} \\ U_{[2]}^{Re} \\ U_{(3)}^{Re} \\ U_i^{Im} \\ U_{(1)}^{Im} \\ U_{[2]}^{Im} \\ U_{(3)}^{Im} \end{bmatrix} = Q^T \begin{bmatrix} 0 \\ 0 \\ F_{[2]}^{Re} \\ 0 \\ F_{[4]}^{Re} \\ 0 \\ 0 \\ F_{[2]}^{Im} \\ 0 \\ F_{[4]}^{Im} \end{bmatrix} = 0 \tag{B.11}$$

References

[1] Bisagni C, Vescovini R. Fast tool for buckling analysis and optimization of stiffened panels. J Aircr 2009;46(6):2041–53.

[2] Johnson Jr R. Design and fabrication of a ring-stiffened graphite-epoxy corrugated cylindrical shell. NASA CR-3026; 1978.

[3] Block DL, Card MF, Mikulas Jr MM. Buckling of eccentrically stiffened orthotropic cylinders. NASA-TN-D-2960; 1965.

[4] Amazigo JC, Hutchinson JW. Imperfection-sensitivity of eccentrically stiffened cylindrical shells. AIAA J 1967;5(3):392–401.
[5] Simitses GJ. General instability of eccentrically stiffened cylindrical panels. J Aircr 1971;8(7):569–75.
[6] Calladine CR. Theory of shell structures. Cambridge University Press; 1989.
[7] Yokozeki T, Takeda S, Ogasawara T, Ishikawa T. Mechanical properties of corrugated composites for candidate materials of flexible wing structures. Compos Part A: Appl Sci Manuf 2006;37(10):1578–86.
[8] Thill C, Etches JA, Bond IP, Potter KD, Weaver PM, Wisnom MR. Investigation of trapezoidal corrugated aramid/epoxy laminates under large tensile displacements transverse to the corrugation direction. Compos Part A: Appl Sci Manuf 2010;41(1):168–76.
[9] Briassoulis D. Equivalent orthotropic properties of corrugated sheets. Comput Struct 1986;23(2):129–38.
[10] Liew KM, Peng LX, Kitipornchai S. Nonlinear analysis of corrugated plates using a FSDT and a Meshfree method. Comput Methods Appl Mech Eng 2007;196(21):2358–76.
[11] Xia Y, Friswell MI, Flores EI. Equivalent models of corrugated panels. Int J Solids Struct 2012;49(13):1453–62.
[12] Ye Z, Berdichevsky VL, Yu W. An equivalent classical plate model of corrugated structures. Int J Solids Struct 2014;51(11):2073–83.
[13] Lamberti L, Venkataraman S, Haftka RT, Johnson TF. Preliminary design optimization of stiffened panels using approximate analysis models. Int J Numer Methods Eng 2003;57(10):1351–80.
[14] Combescure A. Static and dynamic buckling of large thin shells: design procedure, computation tools, physical understanding of the mechanisms. Nucl Eng Des 1986;92(3):339–54.
[15] Combescure A, Pernette E. Linear and nonlinear buckling of discrete supported cooling towers using special axisymmetric shell elements. Nucl Eng Des 1989;111(2):217–25.
[16] Combescure AG. Modeling elastic-plastic buckling of sandwich axisymmetric shells: on the limits of shell models and analytical solutions. Adv Model Simul Eng Sci 2014;1(1):1.
[17] Gusic G, Combescure A, Jullien JF. The influence of circumferential thickness variations on the buckling of cylindrical shells under external pressure. Comput Struct 2000;74(4):461–77.
[18] Steele CR. Asymptotic-numeric solution for shells of revolution. Appl Mech Rev 1995;48(11S):S44–51.
[19] Steele CR. Application of the WKB method in solid mechanics. Mech Today 1976;3:243–95.
[20] Fettahlioglu OA, Steele CR. Asymptotic solutions for orthotropic nonhomogeneous shells of revolution. J Appl Mech 1974;41(3):753–8.
[21] Wittrick WH, Williams FW. Buckling and vibration of anisotropic or isotropic plate assemblies under combined loadings. Int J Mech Sci 1974;16(4):209–39.
[22] Anderson MS, Williams FW, Wright CJ. Buckling and vibration of any prismatic assembly of shear and compression loaded anisotropic plates with an arbitrary supporting structure. Int J Mech Sci 1983;25(8):585–96.
[23] Williams FW, Anderson MS. Incorporation of Lagrangian multipliers into an algorithm for finding exact natural frequencies or critical buckling loads. Int J Mech Sci 1983;25(8):579–84.
[24] Williams FW, Anderson MS, Kennedy D, Butler R, Aston G. VICONOPT-Program for exact vibration and buckling analysis or design of prismatic plate assemblies. NASA CR-181966; 1990.
[25] Singer J, Arbocz J, Weller T. Buckling experiments: experimental methods in buckling of thin-walled structures, vol. 2. New York: Wiley; 2002.
[26] Williams FW. An algorithm for exact eigenvalue calculations for rotationally periodic structures. Int J Numer Methods Eng 1986;23(4):609–22.
[27] Williams FW. Exact eigenvalue calculations for structures with rotationally periodic substructures. Int J Numer Methods Eng 1986;23(4):695–706.
[28] Geymonat G, Müller S, Triantafyllidis N. Homogenization of nonlinearly elastic materials, microscopic bifurcation and macroscopic loss of rank-one convexity. Arch Rational Mech Anal 1993;122(3):231–90.
[29] Triantafyllidis N, Schnaidt WC. Comparison of microscopic and macroscopic instabilities in a class of two-dimensional periodic composites. J Mech Phys Solids 1993;41(9):1533–65.
[30] Triantafyllidis N, Schraad MW. Onset of failure in aluminum honeycombs under general in-plane loading. J Mech Phys Solids 1998;46(6):1089–124.
[31] López Jimnez F, Triantafyllidis N. Buckling of rectangular and hexagonal honeycomb under combined axial compression and transverse shear. Int J Solids Struct 2013;50(24):3934–46.
[32] Bertoldi K, Boyce MC, Deschanel S, Prange SM, Mullin T. Mechanics of deformation-triggered pattern transformations and superelastic behavior in periodic elastomeric structures. J Mech Phys Solids 2008;56(8):2642–68.
[33] Gong L, Kyriakides S, Triantafyllidis N. On the stability of Kelvin cell foams under compressive loads. J Mech Phys Solids 2005;53(4):771–94.
[34] Kittel C, McEuen P. Introduction to solid state physics, vol. 8. New York: Wiley; 1976.
[35] Åberg M, Gudmundson P. The usage of standard finite element codes for computation of dispersion relations in materials with periodic microstructure. J Acoust Soc Am 1997;102(4):2007–13.
[36] Shim J, Shan S, Košmrlj A, Kang SH, Chen ER, Weaver JC, et al. Harnessing instabilities for design of soft reconfigurable auxetic/chiral materials. Soft Matter 2013;9(34):8198–202.
[37] Wang D, Abdalla M. Global and local buckling analysis of grid-stiffened composite panels. Compos Struct 2015;119:767–76.
[38] Virgin LN. Vibration of axially loaded structures, vol. 393. New York: Cambridge University Press; 2007.
[39] Dassault Systèmes Simulia Corp. Abaqus 6.12 Documentation. Providence, RI; 2012.
[40] Daniel IM, Ishai O. Engineering mechanics of composite materials. Oxford: Oxford University Press; 2006.
[41] Hilburger MW, Lovejoy AE, Thornburgh RP, Rankin C. Design and analysis of subscale and full-scale buckling-critical cylinders for launch vehicle technology development. In: 53rd AIAA/ASME/ASCE/AHS/ASC Structures, Structural Dynamics and Materials Conference, Honolulu, HI.